IOP PUBLISHING JOURNAL OF OPTICS
J. Opt. **14** (2012) 075704 (9pp) doi:10.1088/2040-8978/14/7/075704

Grating beam splitting with liquid crystal adaptive optics

J Albero and I Moreno

Departamento de Ciencia de Materiales, Óptica y Tecnología Electrónica, Universidad Miguel Hernández, 03202 Elche, Spain

E-mail: j.albero@umh.es

Received 30 March 2012, accepted for publication 12 June 2012
Published 28 June 2012
Online at stacks.iop.org/JOpt/14/075704

Abstract
We report on the generation of equi-intense light beams from an adaptive point of view. A phase mask is generated and displayed onto a spatial light modulator, in order to divide an incoming light beam into a chosen number of beams. The use of liquid crystal spatial light modulators can introduce polarization into scalar designs as a parameter acting on the output efficiency. We reproduce the modulator optimal designs proposed theoretically in the literature and we add the polarization features. In addition, we compare this with another beam splitting technique, based on spatial multiplexing of phase masks. It spreads as low-level background noise the light concentrated on diffraction orders other than those targeted. We also demonstrate that using polarization with spatial light modulators can improve in some cases the optimal theoretical efficiencies. Experimental results agree with simulations.

Keywords: spatial light modulators, beam splitters, phase gratings, polarization

(Some figures may appear in colour only in the online journal)

1. Introduction

Light addressing and splitting are among the most used functions of diffractive optical elements (DOEs). Over the years, researchers have proposed techniques to distribute an input light beam in N separate beams. Such beam splitters find their application in optical fiber connectors, optical communications, optical image multiplications, spectroscopy and many others [1]. Optical tweezers also use beam splitting to trap simultaneously a certain number of cells, as reported in [2].

Two aspects are relevant when splitting a beam, the overall efficiency (defined as the sum of the normalized intensities of each outgoing light beam [3]) and the intensity ratio between the output beams. Most of the existing techniques allow different intensities on each beam, although equi-intense beams are often considered. A trivial example of $N = 1$ are standard blazed gratings, where the single deflected beam is obtained with an ideal 100% efficiency. Well-known examples of light splitting are duplicators ($N = 2$) and triplicators ($N = 3$), where light is split into two or three beams, respectively, as used for instance in CD and DVD tracking [4]. The binary π-phase grating has been demonstrated to be the scalar duplicator with the maximum overall efficiency $\eta = 8/\pi^2$ [5]. In the early 1970s, Dammann *et al* developed a method to design binary π-phase gratings that create arbitrary N uniformly intense diffraction orders [6]. The Dammann grating producing a triplicator ($N = 3$) has an overall efficiency $\eta = 0.92$. Gori *et al* reported the analytical derivation of the continuous phase profile needed to obtain an optimum scalar triplicator. It led to a maximum overall efficiency of $\eta = 0.926$ [5], which was very near to the upper bound stated in [7]. In the early 1990s, Prongué *et al* proposed a kinoform optimization that led to continuous volume gratings to produce N fan-out elements [8]. Using that method, uniform outgoing beams with high efficiencies can be obtained. A clear summary of the first works in this field can be found in [9]. The method proposed in [8] was extended by Romero and Dickey [10], with some differences on the approach but with nearly the same results. They generalized the methods of the triplicator design in [5] for arbitrary N. The same authors apply their solution to square and hexagonal 2D gratings [11]. These methods are reviewed in [12].

The fabrication of diffractive gratings is based on many different techniques [13–15]. Optimal scalar gratings have been reported at industrial level by Miklyaev *et al* [16]. However, they have not been reproduced with spatial light modulators (SLMs), which are nowadays a meaningful alternative for beam splitting. Although the theoretical efficiencies would be reduced due to the SLM pixelated structure, these devices offer some advantages since they are reconfigurable. Also, it is important to note that liquid crystal SLMs (LC-SLMs) are usually polarization sensitive. That feature must be considered when dealing with diffraction efficiencies. For instance, in a parallel-aligned liquid crystal display (PAL-LCD), such as the one used in this work, the displayed phase mask only modulates the electric field component parallel to the liquid crystal (LC) director axis. The component perpendicular to the LC director is not modulated, thus contributing to the zeroth diffraction order. Therefore, light in higher diffraction orders is linearly polarized parallel to the LC director axis. Examples of SLM beam splitting applications have been reported. In [17], a polarization beam splitter displayed onto a SLM was used to create an off-axis duplicator, where the zeroth and first diffraction orders had equal intensity but different polarization. Similarly, the generation of an off-axis triplicator was demonstrated in [18], where the zeroth and second order had orthogonal polarizations and the first order was elliptically polarized. This was obtained by using a reflective optical architecture that required a double pass through a modulator. These are particular cases of polarization diffraction gratings, a type of element that periodically modifies the state of polarization. Considering the electromagnetic nature of light, such polarization diffraction gratings with subwavelength periods have been designed as a triplicator with theoretical efficiencies of 100% [19].

Another alternative for beam splitting consists of using random mask encoding techniques, where each pixel randomly displays the phase of one of the multiplexed diffractive element. Whereas optimal grating designs can be fabricated with bulk materials [16], the use of SLMs makes possible the spatial multiplexing of phase gratings, which is difficult to generate with other techniques. Random multiplexing of diffractive elements was proposed by Davis *et al* [20] to generate multifocal diffractive lenses. Since then, it has been applied to a variety of DOEs, including diffractive lenses with extended depth of focus [21], multiple optical traps [2] or computer-generated holograms [22].

In this paper, we demonstrate the realization of grating beam splitters onto SLMs and we compare the performances of some of the above-mentioned techniques. While optimal designs show better diffraction efficiency, multiplexed phase profiles eliminate unwanted high diffraction orders (so-called ghost orders). This is especially interesting in the case of the duplicator, since it reproduces the Fresnel biprism and it can be applied for interferometric purposes. In all cases, we show how the non-diffracted polarization component can be used to contribute to the zeroth order, in some cases leading to an improved overall efficiency.

The paper is organized as follows. In section 2, we present the techniques to be encoded on the SLM, giving the principles of those found in the literature and describing the random multiplexing technique. The role of polarization is discussed as well. Section 3 is devoted to simulations, whereas section 4 discusses the experimental results. Conclusions are given in section 5.

2. Beam splitting techniques

2.1. Optimal beam splitting

Among the previously mentioned studies on optimal beam splitting, the work done by Romero and Dickey [10–12] provides an extensive study. In [10], the goal consists of finding a phase-only function $\exp[\mathrm{i}\phi(x)]$ that produces a set of diffraction orders with a defined relative intensity (usually selected to be equal), with the maximum overall efficiency. Let a_k represent the kth Fourier coefficient of $\exp[\mathrm{i}\phi(x)]$,

$$a_k = \frac{1}{2\pi}\int_{-\pi}^{\pi} \exp[\mathrm{i}\phi(x)]\exp[-\mathrm{i}kx]\,\mathrm{d}x, \quad k = 0, \pm1, \pm2, \ldots. \tag{1}$$

Following [12], the optimal phase function can be found as

$$\exp[\mathrm{i}\phi(x)] = \frac{s(x, \underline{\alpha}, \underline{\mu})}{|s(x, \underline{\alpha}, \underline{\mu})|} \tag{2}$$

where $\underline{\alpha}$ and $\underline{\mu}$ are two sets of optimization parameters α_k and μ_k, which represent the phase and amplitude of each component of the function $s(x, \underline{\alpha}, \underline{\mu})$ respectively, i.e.

$$s(x, \underline{\alpha}, \underline{\mu}) = \sum_{k=-m}^{m} \mu_k \exp[\mathrm{i}\alpha_k]\exp[\mathrm{i}kx]. \tag{3}$$

The overall diffraction efficiency can be defined as

$$\eta = \frac{\sum_{k=-m}^{m} |a_k|^2}{\sum_{k=-\infty}^{\infty} |a_k|^2}. \tag{4}$$

The problem is solved when the phase $\phi(x)$ that maximizes η is obtained, constrained to a certain relative proportion among the intensities $|a_k|^2$ of the target orders (the diffractive orders that constitute N). For the sake of simplicity, we focus on equi-intense fan-out beams. The optimal solution is reached in two steps. First, the phases α_k associated to the kth orders are computationally sought to maximize η, regardless of the intensities $|a_k|^2$, i.e. $\mu_k = 1$ is selected in this first step. Second, the amplitudes μ_k are added as variables in order to obtain diffracted orders with the same intensity. Although the phase values obtained in the first step are sometimes equivalent to those obtained in the second step, they may vary, but they serve as an initial guess for the algorithm to find the optimal solution.

The solution of this problem generates $N = 2m + 1$ diffracted orders if N is odd, and $N = 2m$ diffracted orders if N is even. If the designed beam splitter is symmetric, the optimal solution can be assumed to be symmetric as well, so that $\alpha_k = \alpha_{-k}$ and $\mu_k = \mu_{-k}$. This reduces the number of parameters to be determined and thus the

Figure 1. Scheme of the technique used to generate a multiplexed duplicator with random binary amplitude masks. $\pm\phi(x)$ represent the two opposite signed linear phases yielding the two diffraction orders; A and $\bar{A}$ represent two complementary binary random amplitude masks.

associated computational effort. Although an asymmetric optimal solution could exist for a symmetric problem, the best solution under the symmetry assumption still provides properly high efficiencies. Moreover, it was demonstrated that the first α_k and μ_k could be fixed to 0 and 1, respectively [10]. Different cases and their corresponding values can be found in [12]. For instance, the optimal triplicator with target orders 0 and ±1 is given by [10]

$$\tan[\phi(x)] = 2\mu\cos(x) \qquad \text{with } \mu \approx 1.32859, \tag{5}$$

in agreement with the optimal design first presented in [5].

2.2. Beam splitting by multiplexed phase masks

Another option to generate the same type of grating beam splitters that can be easily implemented in SLMs is the random multiplexing technique. For simplicity, the process is introduced for two-profiles multiplexing and it will be extended later to multiplex N phase profiles. Let us consider a matrix D of $n \times m$ elements

$$D = (d_{xy}); \qquad x = 1, \ldots, n \quad y = 1, \ldots, m \tag{6}$$

where each d_{xy} is a discrete random variable in the range $[a, b]$ with uniform probability distribution. To multiplex two phase profiles, we can define an amplitude mask as a binary amplitude random array $A(x, y)$ as

$$A(x,y) = \begin{cases} 1 & \text{if } d_{xy} \geq \beta \\ 0 & \text{otherwise} \end{cases} \quad a \leq \beta \leq b, \tag{7}$$

where x and y correspond here to the spatial coordinates of the SLM pixels and β is the threshold value that weights the distribution of each amplitude value. Different weights can be applied to each amplitude value by adjusting the value of β. The condition for an even amplitude distribution among the pixels in $A(x, y)$ is

$$\beta = \frac{b-a}{2}. \tag{8}$$

Once the amplitude random mask is obtained, it is multiplied by one of the phase profiles to be multiplexed. The second phase profile is multiplied by the complementary binary amplitude random array $\bar{A}(x, y)$ (which is simply an exchange of 0 by 1 and vice versa at each pixel). The sum of both products results in the randomly multiplexed phase mask $\Phi(x)$.

In the case of grating beam splitters, the phase masks to be multiplexed correspond to linear phase patterns (blazed gratings). For instance, the symmetrical duplicator can be simply created by randomly multiplexing two opposite continuous phase ramps, i.e. two opposite blazed gratings, defined as $\exp[\pm i2\pi x/p]$, where p is the period of the grating. This is illustrated in figure 1, where two periods of the blazed gratings are shown. The resulting phase-only mask can be expressed as

$$\exp(i\Phi(x)) = A(x,y)\exp\left(i2\pi\frac{x}{p}\right) + \bar{A}(x,y)\exp\left(-i2\pi\frac{x}{p}\right). \tag{9}$$

If condition (8) is satisfied, two equally intense ±1 diffraction orders are generated. Note that this duplicator follows the idea of the Fresnel biprism, where the bases of two equal prisms are brought together forming an isosceles triangle shape in order to create two opposite continuous phase changes. When a plane wavefront enters the biprism, each prism will refract half of the incoming light if the beam is well centered, creating two separate virtual coherent images of the original source. Such biprisms are used in, e.g. stereoscopic cameras [22]. Here, as the patterns to be multiplexed are basically gratings extended all over the image, it prevents us from needing a precisely centered beam as with a bulk Fresnel biprism. As mentioned, a binary π-phase grating can reproduce these effects with optimal overall efficiency. However, a certain light intensity appears concentrated on ghost diffraction orders. By spatial multiplexing, a quasi-pure duplicator with a low amount of background noise is obtained, as we show in the following sections.

The process can be extended to multiplex more phase profiles by dividing the range $[a, b]$ in N subintervals and defining different random amplitude masks as

$$A_q(x,y) = \begin{cases} 1 & \text{if } d_{xy} \in [\beta_q, \beta_{q+1}] \\ 0 & \text{otherwise } \forall q = 1, \ldots, N-1 \end{cases} \quad a \leq \beta_q \leq \beta_{q+1} \leq b \tag{10}$$

In theory, N phase profiles should be multiplexed to split a beam into N beams. Therefore $q_{\max} = N - 1$ must be set. Similarly as in (7), if the subintervals are equally distributed in the range $[a, b]$, each phase profile will have the same weight, i.e. the number of pixels corresponding to each phase profile after multiplexing will be the same. It must be noted that the more phase profiles multiplexed, the lower the overall efficiency.

In [2], this method was applied to multiplex phase profiles and generate multiple optical traps. Here, we apply the same concept and we multiplex blazed gratings in order to generate grating beam splitters. By properly setting the period of the blazed gratings, one can reach as many fan-out elements as desired. Subsequently, perfectly symmetric beam splitting can

be easily obtained. Similarly, the period provides the degree of freedom to create and control asymmetry when needed. Moreover, spatial multiplexing linked to the SLM adaptive properties opens a wide range of degrees of freedom. As an example, 2D spatial offset of the beams can be achieved by just introducing both x and y spatial coordinates in the phase ramp definition.

It is important to note that, although elements could be fairly freely placed in the Fourier plane, the highest efficiencies are obtained around the optical axis. This is due to the fact that the farther the element diffracts from the zeroth order, the shorter the period of its associated grating. It implies a loss of resolution in the phase ramp due to quantization. If L is the number of phase levels, the maximum efficiency of a blazed grating is limited by [23]

$$\left[\frac{\sin(\pi/L)}{\pi/L}\right]^2. \tag{11}$$

Nevertheless, this effect can be partially compensated with the proper selection of the values β_k in equation (10) to change the weight of each order.

2.3. Control of the zeroth order by polarization

The use of LC-SLMs adds the polarization state as an additional parameter to be considered. We deal here with a PAL-LCD. If the input polarization is linear and oriented parallel to the LC director axis, this SLM acts as a scalar diffractive element capable of reproducing phase masks, since this polarization state is fully modulated. However, if the input polarization is different, non-modulated light is sent towards the zeroth order. Thus, the intensity of the latter (and subsequently its absence) can be controlled by properly adjusting the polarization state of the input beam. With our symmetric beam splitting approach, the presence or absence of the zeroth order is the key to switch from an even to an odd number of beams. By rotating the input linear polarization an angle θ with respect to the LC director axis, a fraction $\sin^2\theta$ of the incoming intensity is not modulated and it is thus directed to the zeroth diffraction order, whilst a fraction $\cos^2\theta$ is fully modulated, in accordance with scalar diffraction efficiency (equation (4)). A grating beam splitter can be designed without zeroth diffraction order (thus providing more efficiency to the rest of the orders) and the angle θ can be found so that the zeroth order has the same intensity as the rest of target orders. This is obtained by setting

$$\theta = \arctan\sqrt{\frac{\eta}{N}}, \tag{12}$$

where η/N is the efficiency of a single fan-out element of the split beam. Subsequently, the zeroth order has orthogonal polarization with respect to the side orders. This odd N generation can be extended to optimal beam splitter generation, as will be shown.

Additionally, polarization is a very efficient way to generate the zeroth order when using multiplexed phase masks. It reduces the amount of background noise and the efficiency is obviously higher than multiplexing an additional phase profile to generate the zeroth order. Moreover, the main interest of polarization control lies in rapid switching between even N and $N+1$. For instance, ferroelectric liquid crystal modulators can be used to switch between polarization states much faster than switching phase profiles on the LC screen [24].

3. Simulations

Prior to testing the ability of SLMs for beam splitting purposes, we simulated the configurations in order to establish some parameters, such as the expected overall efficiencies α_k and μ_k, of the optimal solutions to be tested, and the angle θ to generate an odd N by polarization. The Fourier transform of the designed phase-only masks is calculated and the profile of the diffracted orders normalized intensity pattern is reproduced in each case.

Figures 2(a) and (b) compare the diffraction order profiles generated by a binary π-phase-only grating, i.e. the optimal duplicator (figure 2(a)) and the random duplicator (figure 2(b)). As is shown for the π-phase binary grating, the zeroth order vanishes and most of the intensity (81%) is found at the $\pm$1st orders, but also higher odd orders present a considerable intensity (e.g. $|a_{\pm3}|^2 = 0.046$). When the spatial multiplex is used, higher orders are fully eliminated, but this occurs at the expense of decreasing the overall efficiency due to the appearance of low background noise. This is due to the effect of the random amplitude mask [25]. To notice the noise, a logarithmic scale must be applied to the zoomed representation (inset of figure 2(b)).

In figures 2(c)–(f), we reproduce the simulation results for differently generated triplicators. When the optimal scalar triplicator (equation (5)) is considered (figure 2(c)), the efficiency is the highest, $\eta = 0.926$. Additional diffraction orders are present, having the most intense efficiencies at $|a_{\pm2}|^2 = 0.02$. If the triplicator is generated by the random multiplexed method, the efficiency decreases to $\eta = 0.340$, but in exchange the ghost orders intensity is again spread into background noise and only three main spots are relevant (figure 2(d)). The average noise intensity is around 1×10^{-10}, with maximum peaks around 8×10^{-9}. This efficiency can be much improved, up to $\eta = 0.602$, if the multiplexed duplicator is turned into a triplicator by polarization (figure 2(e)). This is obtained by rotating the input polarization by $\theta = 26.61°$. This triplicator still shows no ghost orders while providing a considerable increase of efficiency compared to figure 2(d). Finally, an intermediate case is obtained when an optimal duplicator (the π-phase grating in figure 2(a)) is similarly turned into a triplicator by polarization (figure 2(f)). The input polarization is now rotated by $\theta = 32.48°$ and the efficiency is $\eta = 0.827$. Ghost orders are more intense in this case than in figure 2(c). However, they appear at higher indices ($k = \pm3$, $\pm5, \ldots$).

Table 1 summarizes the simulated overall efficiencies of each case up to $N = 11$ for optimal and multiplexed phase masks. In the optimal solutions, Table 1 gives the values of α_k and μ_k calculated in our conditions as well. When

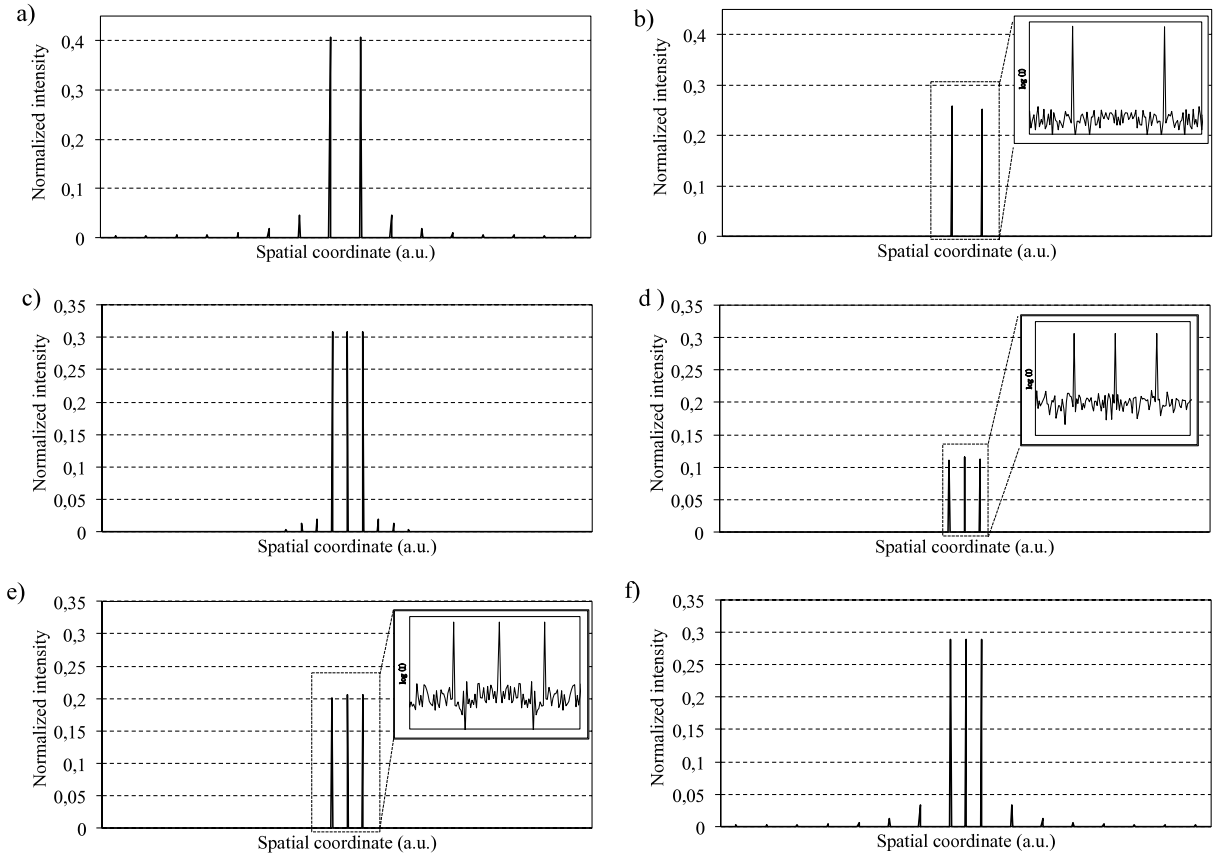

Figure 2. Comparison of numerical simulations, (a) a standard π-phase-only binary grating; (b) spatially multiplexed ± 1 duplicator; (c) optimal triplicator proposed in [5]; (d) spatially multiplexed 0, ± 1 triplicator; (e) spatially multiplexed ± 1 duplicator plus polarization zeroth order; (f) triplicator obtained by polarization over the optimal duplicator. Insets in (b), (d) and (e): logarithmic scale of the zone of interest for better visibility of the background noise.

$N > 7$, the multiplexing technique offers too low efficiency to be considered as a relevant choice. Table 1 also lists the overall efficiency for odd N when it is generated with an optimal solution for even N and the zeroth order is generated by polarization rotation. Note that the optimal efficiencies in table 1 are slightly different to those found in the literature. This is mainly due to two reasons. First, our simulations take into account quantization, present when SLMs are used. Namely, each 2π period is assumed in steps of 255 values to match the typical gray-scale used to address SLMs. Second, and especially relevant for even number of elements N, the target orders considered here are different. It is usual to consider equidistant-spot beam splitters, so that light appears in the $k = \pm 1, \pm 3, \pm 5, \ldots$ orders. As our aim is using them as the basis for beam splitters with odd numbers of elements, it is more convenient to have light appearing in consecutive orders, i.e. $k = \pm 1, \pm 2, \pm 3, \ldots$. Therefore, when the zeroth order is present, all orders are equidistant. From the results in table 1 it can be concluded that optimal designs give, as expected, the highest efficiencies. Let us remark that a situation where the highest efficiency is not obtained by the optimal scalar beam splitter is possible. The optimal $N = 4$ grating plus the additional zeroth order by polarization gives higher efficiency than the optimal $N = 5$ grating. Since the optimal α_k and μ_k are the result of a numerical computation, the algorithm could converge to a local maximum instead of a global maximum. Although the efficiencies obtained by optimal gratings plus polarization are lower, the difference is noticeable only at the second decimal position. In applications where efficiency is not a critical parameter, the zeroth order obtained by polarization could be preferred, since it has the added value of providing fast switching between even N and $N + 1$.

4. Experimental realization

The setup used in the experiments is shown in figure 3. A parallel-aligned reflective Hamamatsu LCOS-SLM X10468-01 series acts as a programmable waveplate. The SLM is illuminated with a tunable Ar laser emitting at a wavelength $\lambda = 514$ nm. The SLM is adjusted to produce a maximal phase modulation of 2π at the operating wavelength. A CCD camera with a resolution of 1392 pixels $\times$ 1040 pixels (Basler scA1390-17fc) is used to capture the images of the far field diffraction pattern. Prior to illuminating the SLM, the laser light is expanded with a spatial filter and collimated with a lens. An input linear polarizer is placed right before the SLM.

Table 1. Overall efficiencies η of the different beam splitter encodings and the values of α_k and μ_k of each optimal encoding. We assume $\alpha_k = \alpha_{-k}$ and $\mu_k = \mu_{-k}$ and the first α_k and μ_k equal to 0 and 1, respectively.

N	Target orders	Multiplexed	Optimal	Optimal + polarization
2	±1	0.502	0.811 π-phase grating	—
3	0, ±1	0.602	0.926 $\alpha = (\pi/2)$ $\mu = (1.329)$	0.867
4	±1, ±2	0.256	0.945 $\alpha = (1.588)$ $\mu = (1.051)$	—
5	0, ±1, ±2	0.296	0.920 $\alpha = (-\pi/2, \pi)$ $\mu = (0.448, 0.889)$	0.961
6	±1, ±2, ±3	0.167	0.916 $\alpha = (1.632, 3.198)$ $\mu = (0.552, 1.188)$	—
7	0, ±1, ±2, ±3	0.191	0.968 $\alpha = (-1.191, 1.764, 0.670)$ $\mu = (1.272, 1.427, 1.241)$	0.940
8	±1, ±2, ±3, ±4	—	0.913 $\alpha = (1.743, 4.542, -1.310)$ $\mu = 1.729, 1.391, 1.653$	—
9	0, ±1, ±2, ±3, ±4	—	0.993 $\alpha = (0.662, 5.462, 3.022, 1.268)$ $\mu = (1.053, 1.018, 0.980, 1.141)$	0.931
10	±1, ±2, ±3, ±4, ±5	—	0.930 $\alpha = (5.078, 4.999, 2.735, 3.765)$ $\mu = (1.045, 1.018, 0.980, 1.141)$	—
11	0, ±1, ±2, ±3, ±4, ±5	—	0.975 $\alpha = (0.579, 4.906, 2.975, 5.485, 4.554)$ $\mu = (0.579, 4.906, 2.975, 5.485, 4.554)$	0.938

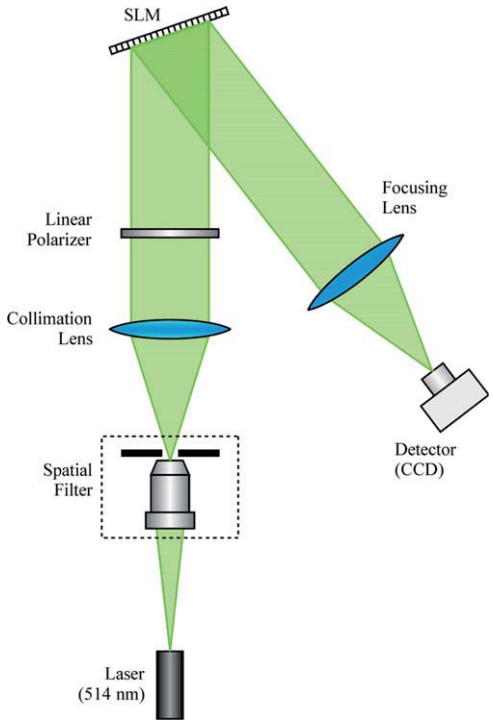

Figure 3. Experimental setup for beam splitting with an SLM.

Polarization is controlled by rotating the input linear polarizer an angle θ with respect to the LC director axis.

4.1. Beam splitters

Figure 4 shows the Fourier plane experimental images of the simulated configurations up to $N = 7$. Two options are displayed, the optimal design and the multiplexed design. For odd N, an additional case is the optimal mask for even N plus the zeroth order introduced by polarization rotation. Table 2 lists the calculated angles θ to obtain odd N by polarization, both using optimal encoding and spatial multiplexing. For the image acquisition, the minimum input intensity is set to $I_{\text{in}} = 1$ a.u. to achieve good visibility of the diffracted orders with the optimal gratings. Note that I_{in} must be increased by the factor marked in figure 4 to achieve comparable spot intensities when displaying the multiplexed profiles on the SLM. The results in the first and second columns for optimal encodings show how the light not contributing to target orders appears in ghost orders, e.g. $k = \pm3$ for $N = 2$, $k = \pm2$ for $N = 3$, $k = \pm4$ for $N = 5$ or the zeroth order for $N = 6$. When beam splitting is obtained by random multiplexing, some noise can be noticed if the intensity is very high, as in $N = 4$ and 6. As an example, experiments revealed overall experimental efficiencies $\eta = 0.47$ for the multiplexed duplicator encoding and $\eta = 0.58$ when adding the zeroth order by polarization, these values being very close to the simulations. Note that the SLM pixelated structure introduces additional efficiency losses. These experimental values are normalized to the intensity going onto the zeroth diffraction

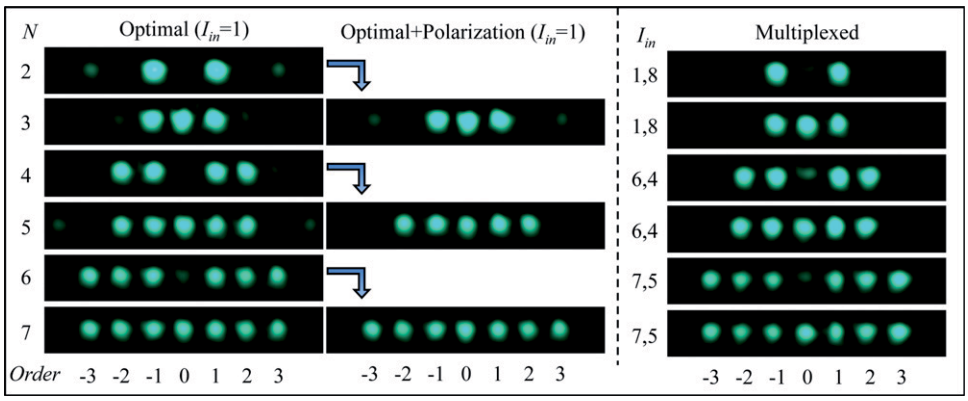

Figure 4. Images of the experimental diffracted orders obtained when the grating beam splitters are displayed onto a PAL-SLM. The intensities I_{in} are expressed in arbitrary units.

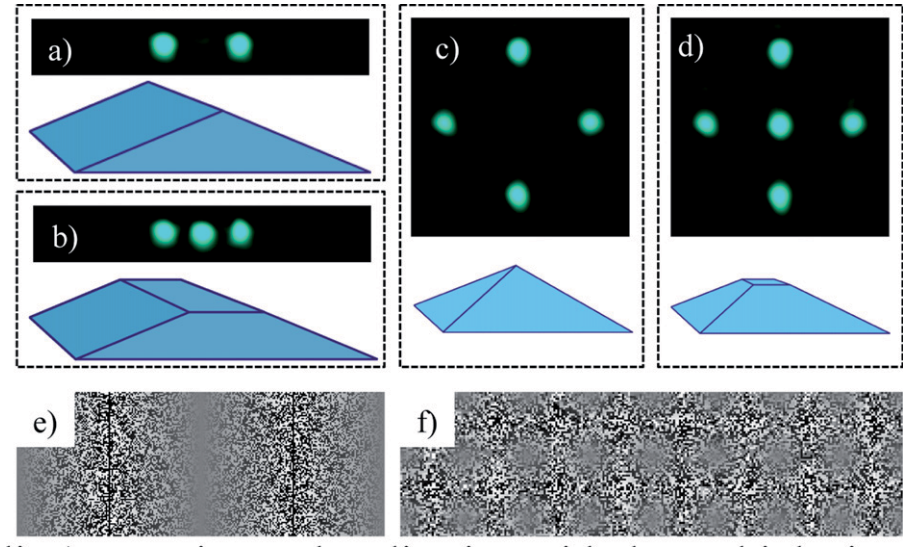

Figure 5. Experimental realization with the multiplexing + polarization method, and their corresponding analogous prism sketch: (a) duplicator; (b) triplicator; (c) four-spot square distribution; (d) five-spot distribution; (e) phase encoded onto the SLM to generate (a) and (b); (f) phase encoded onto the SLM to generate (c) and (d).

Table 2. Calculated θ angles to convert even N into odd N with the zeroth diffracted order.

N	Optimal encoding (deg)	Multiplexed encoding (deg)
2–3	32.48	26.61
4–5	25.23	14.08
6–7	20.34	9.48

order generated by the 2D SLM pixel matrix, which acts as a diffractive grid.

4.2. Prism analogies

Since duplicator and triplicator configurations are most commonly used, let us focus on them in this subsection to show some of the additional features that their realization with SLMs offer. We will deal with those obtained by random spatial multiplexing since the presence of ghost orders strongly affects interference fringes.

These elements basically reproduce refractive prisms. For instance, the duplicator can be considered equivalent to a Fresnel biprism. But the realization with SLMs offers some relevant advantages. When using the random multiplexing technique, the two linear phase patterns (blazed gratings) are extended all over the display and prevent a precise centering. The generated first orders have the same intensity and they are symmetric with respect to the absent zeroth central order. Figures 5(a) and (b) show the images of both the duplicator and triplicator configurations and a scheme of the equivalent refractive prism.

As an example of the versatility offered by their implementation in SLMs, we multiplexed the duplicator phase profile with a 90° rotation of itself, thus creating a pyramid-like prism. Bulk versions of this pyramid-like prism are used, for instance, in pyramid wavefront sensors [26] and in pyramid phase microscopy [27]. These pyramids are analogous to a four sector phase mask, each of them with a blazed grating. Figure 5(c) shows the experimental generation of these four orders. Similarly, we rotated the

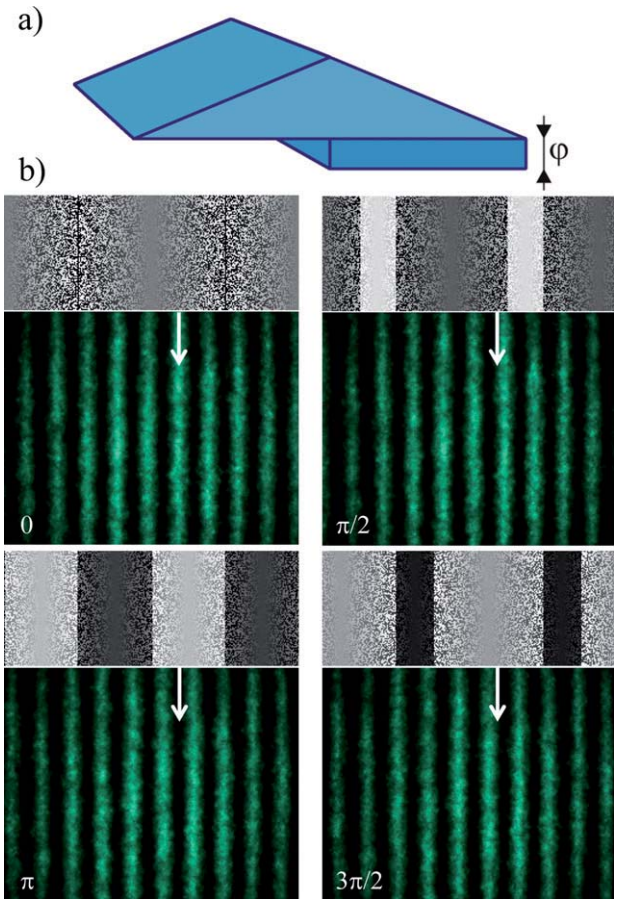

Figure 6. (a) Sketch of the prism variation needed to produce the phase variation on one of the sides; (b) interference fringes created by the multiplexed duplicator (biprism) in the close region to the SLM. Phase steps of $\varphi = \pi/2$ are added to one of the phase gratings.

input polarization $\theta = 13.3°$ to allow some light to go to the zeroth order and an equi-intense five-spot distribution was obtained (figure 5(d)). A few periods of the phase gratings encoded onto the SLM for all four cases in figures 5(a)–(d) are represented in figures 5(e) and (f). Note that optimal designs for these two-dimensional gratings are also provided in [11], although we present here the results with the multiplexing method for simplicity.

Fresnel biprisms find applications in interferometry. Here, we use the multiplexed duplicator analog of the biprism where the SLM adaptability provides additional performance compared to glass biprisms. This is shown in figure 6, where the focusing lens was removed, the camera was located in a plane closer to the SLM and a low spatial frequency duplicator was displayed. The light beam presents the interferometric pattern characteristic of a Fresnel biprism. This SLM-based biprism has additional features. Let us now consider a situation where one of the two blazed gratings is fixed, whereas the other one is spatially displaced in the direction of the phase variation. Each displacement step is equivalent to adding a constant phase to the blazed grating, i.e. a displacement of the interference fringes after the biprism. The bulk version of the biprism would require an additional piece

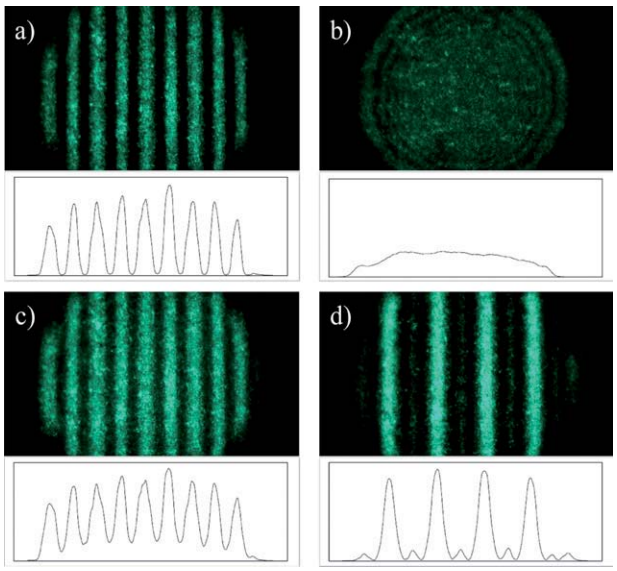

Figure 7. Interference patterns in the close region to the SLM with the triplicator configuration and their 2D intensity profiles (in arbitrary units): (a) analyzer parallel to the LC director axis, (b) analyzer perpendicular to the SLM director axis, (c) without analyzer, (d) analyzer at 45° to the LC director axis to force three-beam interference.

of glass in one of the prisms, as sketched in figure 6(a). On top of each item of figure 6(b) we see the two periods of the displayed phase masks, where the phase of one of the blazed gratings is increased in steps of $\varphi = \pi/2$. The corresponding captured interference pattern is shown as well, where the fringe displacement is clearly visible. The arrows mark the original starting position to show the displacement.

If now we rotate the input polarization by the angle θ to produce the polarization triplicator, three-beam interference can be produced. However, as the polarization of the $+1$ and -1 diffraction orders is perpendicular to the polarization of the zeroth order, an analyzer must be placed after the SLM and oriented at 45° with respect to the LC director axis. Figure 7 shows the patterns captured by the camera as the analyzer is rotated, together with the associated intensity profile. Figure 7(a) reproduces the duplicator scheme since the analyzer is parallel to the LC director, and therefore the zeroth order is not transmitted. In figure 7(b), the analyzer is rotated to be perpendicular to the LC director axis and thus only the zeroth order is transmitted and the interference disappears. If the analyzer is removed, both previous patterns with orthogonal polarizations incoherently overlap (figure 7(c)), resulting in the two-beam interference pattern with additional background light. Finally, in figure 7(d), the analyzer is set at 45° with respect to the LC director axis, all three beams are projected in this polarization axis with equal intensity and the three-beam interference occurs.

5. Conclusions

In conclusion, we have analyzed different ways to generate grating beam splitters onto liquid crystal SLMs. We have experimentally implemented optimal designs onto SLMs and

compared them with random multiplexed methods. The first show optimal diffraction efficiency but ghost orders are also present. The second type is valid when a low number of beams is required. Although less efficient, light on the ghost orders is distributed as some background noise. We have also included the polarization control over the zeroth order, since we employ a parallel-aligned liquid crystal SLM. The use of such devices makes it possible to introduce new optimal designs where the zeroth order is absent in the scalar grating, but it is included by rotation of the input polarization. This technique provides fast switching from an even number of target orders N to $N + 1$. Polarization control of the zeroth order in some cases increases the efficiency over the theoretical optimal values. Following the principle of a Fresnel biprism and multiplexing two phase masks onto a SLM we have reproduced interferometric patterns. The reconfigurable characteristic of the SLM is shown to be valuable for interferometry. Experimental results have been presented in all cases, including various optimal designs.

Acknowledgments

This work received financial support from Ministerio de Ciencia e Innovación from Spain (ref. FIS2009-13955-C02-02) JA acknowledges the financial support from Ministerio de Educación of Spain through the Programa Nacional de Movilidad de Recursos Humanos del Plan Nacional de I+D+i 2008–2011. The authors are very grateful to Professor Don Cottrell from San Diego State University for allowing the use of *Coherent Optics* software.

References

[1] Aagedal H, Wyrowski F and Schmid M 1997 *Diffractive Optics for Industrial and Commercial Applications* ed J Turunen and F Wyrowski (Berlin: Akademie Verlag) p 165

[2] Montes-Usategui M, Pleguezuelos E, Andilla J and Martín-Badosa E 2006 Fast generation of holographic optical tweezers by random mask encoding of Fourier components *Opt. Express* **14** 2101–7

[3] Moreno I, Iemmi C, Márquez A, Campos J and Yzuel M J 2004 Modulation light efficiency of diffractive lenses displayed in a restricted phase-mostly modulation display *Appl. Opt.* **43** 6278–84

[4] Shih H and Li B 2007 Diffraction grating with dual modes for two-wavelength rewritable optical pickup heads *IEEE Trans. Magn.* **43** 900–2

[5] Gori F, Santarsiero M, Vicalvi S, Borghi R, Cincotti G, Di Fabrizio E and Gentili M 1998 Analytical derivation of the optimum triplicator *Opt. Commun.* **157** 13–6

[6] Dammann H and Görtler K 1971 High-efficiency in-line multiple imaging by means of multiple phase holograms *Opt. Commun.* **3** 312–5

[7] Krackhardt U, Mait J N and Streibl N 1992 Upper bound on the diffraction efficiency of phase-only fanout elements *Appl. Opt.* **31** 27–37

[8] Prongué D, Herzig H P, Dändliker R and Gale M T 1992 Optimized kinoform structures for highly efficient fan-out elements *Appl. Opt.* **31** 5706–11

[9] Mait J N 1997 Fourier array generators *Micro-optics. Elements, Systems and Applications* ed H P Herzig (London: Taylor and Francis) pp 293–324

[10] Romero L A and Dickey F M 2007 Theory of optimal beam splitting by phase gratings. I. One-dimensional gratings *J. Opt. Soc. Am.* A **24** 2280–95

[11] Romero L A and Dickey F M 2007 Theory of optimal beam splitting by phase gratings. II. Square and hexagonal gratings *J. Opt. Soc. Am.* A **24** 2296–312

[12] Romero L A and Dickey F M 2010 The mathematical theory of laser beam-splitting gratings *Prog. Opt.* **54** 319–86

[13] Stern M B 1997 Binary optics fabrication *Micro-optics. Elements, systems and Applications* ed H P Herzig (London: Taylor and Francis) pp 53–86

[14] Gale M T 1997 Direct writing of continuous-relief micro-optics *Micro-optics. Elements, systems and applications* ed H P Herzig (London: Taylor and Francis) pp 87–126

[15] Gomez-Varela A I, Castelo A, Gomez-Reino C, de la Fuente X and Flores-Arias M T 2010 Diffractive gratings fabrication on glass with a laser Nd:YVO4 *Opt. Pura Appl.* **43** 95–9

[16] Miklyaev Y V, Imgrunt W, Bizjak T, Aschke L, Lissotschenko V N, Pavelyev V S and Kachalov D G 2010 Novel continuously shaped diffractive optical elements enable high efficiency beam shaping *Proc. SPIE* **7640** 764024

[17] Davis J A, Adachi J, Fernández-Pousa C R and Moreno I 2001 Polarization beam splitters using polarization diffraction gratings *Opt. Lett.* **26** 587–9

[18] Fernández-Pousa C R, Moreno I, Davis J A and Adachi J 2001 Polarization diffraction-grating triplicators *Opt. Lett.* **26** 1651–3

[19] Tervo J and Turunen J 2000 Paraxial-domain diffractive elements with 100% efficiency based on polarization gratings *Opt. Lett.* **2** 785–6

[20] Davis J A and Cottrell D M 1994 Random mask encoding of multiplexed phase-only and binary phase-only filters *Opt. Lett.* **19** 496–8

[21] Iemmi C, Campos J, Escalera J C, López-Coronado O, Gimeno R and Yzuel M J 2006 Depth of focus increase by multiplexing programmable diffractive lenses *Opt. Express* **14** 10207–19

[22] Lee D H and Kweon I S 2000 A novel stereo camera system by a biprism *IEEE Trans. Robot. Autom.* **16** 528–41

[23] Kuittinen M and Herzig H P 1995 Encoding of efficient diffractive microlenses *Opt. Lett.* **20** 2156–8

[24] Martinez A, Beaudoin N, Moreno I, Sanchez-López M M and Velásquez P 2006 Optimization of the contrast ratio of a ferroelectric liquid crystal optical modulator *J. Opt. A: Pure Appl. Opt.* **8** 1013–8

[25] Rhodes W T and McMeekin M S 1994 Diffraction efficiency of random binary-amplitude diffracting screens *Appl. Opt.* **33** 7569–71

[26] Burvall A, Daly E, Chamot S R and Dainty C 2006 Linearity of the pyramid wavefront sensor *Opt. Express* **14** 11925–34

[27] Iglesias I 2011 Pyramid phase microscopy *Opt. Lett.* **36** 3636–8